Scientific Research Publishing

Journal of Quantum Information Science, 2024, 14, 29-51
https://www.scirp.org/journal/jqis
ISSN Online: 2162-576X
ISSN Print: 2162-5751

Entanglement and Volume Monogamy Features of Permutation Symmetric *N*-Qubit Pure States with *N*-Distinct Spinors: GHZ and $W\bar{W}$ States

Sudha[1,2], Alevoor Raghavendra Usha Devi[2,3], Akshata Shenoy Hejamadi[4], Hosapete Seshadri Karthik[4], Humera Talath[3], Bada Palaiah Govindaraja[1], Attipat Krishnaswamy Rajagopal[2]

[1]Department of Physics, Kuvempu University, Shimoga, India
[2]Inspire Institute Inc., Alexandria, Virginia, USA
[3]Department of Physics, Bangalore University, Bangalore, India
[4]International Centre for Theory of Quantum Technologies, University of Gdánsk, Gdánsk, Poland
Email: tthdrs@gmail.com, ushadevi@bub.ernet.in, akshata.shenoy@ug.edu.pl, attipat.rajagopal@gmail.com

How to cite this paper: Sudha, Usha Devi, A.R., Hejamadi, A.S., Karthik, H.S., Talath, H., Govindaraja, B.P. and Rajagopal, A. K. (2024) Entanglement and Volume Monogamy Features of Permutation Symmetric *N*-Qubit Pure States with *N*-Distinct Spinors: GHZ and $W\bar{W}$ States. *Journal of Quantum Information Science*, **14**, 29-51.
https://doi.org/10.4236/jqis.2024.142003

Received: November 30, 2023
Accepted: April 4, 2024
Published: April 7, 2024

Abstract

We explore the entanglement features of pure symmetric *N*-qubit states characterized by *N*-distinct spinors with a particular focus on the Greenberger-Horne-Zeilinger (GHZ) states and $W\bar{W}$, an equal superposition of W and obverse W states. Along with a comparison of pairwise entanglement and monogamy properties, we explore the geometric information contained in them by constructing their canonical steering ellipsoids. We obtain the volume monogamy relations satisfied by $W\bar{W}$ states as a function of number of qubits and compare with the maximal monogamy property of GHZ states.

Keywords

Permutation Symmetric States, Monogamy, Pairwise Entanglement

1. Introduction

Permutation symmetric multiqubit states form an important class among quantum states due to their experimental significance and mathematical elegance [1]-[7]. The well-known Greenberger-Horne-Zeilinger (GHZ) [8], W, and Dicke states [9], belong to this class. Mathematical simplicity in addressing pure symmetric *N*-qubit states is owing to the fact that they are confined to the $N+1$ dimensional subspace of the 2^N dimensional Hilbert space. The $N+1$ dimensional subspace is the maximal multiplicity space of the collective angular momentum

space of N-qubits with Dicke states [9], the common eigenstates of the squared collective angular momentum operator $\hat{J}^2$ and its z-component J_z forming its basis. In 1932 Majorana [10] proposed an elegant geometrical visualization for pure symmetric N-qubit states as a constellation of N-points on the Bloch sphere S^2. The representation of pure symmetric multiqubit states in terms of constitutent N-qubits (spinors) is called *Majorana representation* [10]. Majorana geometric representation has found several significant applications in quantum information processing [11] [12] [13] [14].

Quantum steering ellipsoid [15] offers a novel geometric picturization of two-qubit states and is useful in understanding quantum correlations such as non-locality, entanglement [16] [17] [18] [19] and quantum discord [16] [17]. The set of all Bloch vectors to which one of the qubits of a two-qubit system can be "steered" when all possible measurements are carried out on the other qubit correspond to *quantum steering ellipsoid* [15]. It has been identified that the volume of the steering ellipsoids [15] corresponding to the two-qubit subsystems of an N-qubit state, $N \geq 3$, effectively captures monogamy properties of the state [18] [20]. Milne *et al.* [18] proposed a monogamy relation, in terms of the volumes of the quantum steering ellipsoids of two-qubit subsystems of a 3-*qubit pure state* which is stricter than the Coffman-Kundu-Wootters (CKW) monogamy relation [21]. A volume monogamy relation satisfied by pure as well as mixed N-qubit states has been obtained in [20] and is helpful in quantifying the shareability properties of the N-qubit state.

The steering ellipsoid of a two-qubit state that has attained a canonical form under suitable local operations on *both the qubits* is the so-called *canonical steering ellipsoid* [22] [23] [24] and provides another geometric representation of a two-qubit state. The canonical steering ellipsoid of any two-qubit state is shown to have only two distinct forms [24] and provide a much simpler geometric picture representing two-qubit states.

The volume monogamy relations for permutation symmetric 3-qubit pure states with two and three distinct spinors are established in [25] using the features of their respective steering ellipsoids. The canonical steering ellipsoids of the entire class of permutation symmetric N-qubit states with two distinct spinors are obtained in [26] and the nature of the volume monogamy relation with increasing N is analyzed [26]. In addition, the obesity of the steering ellipsoids is made use of to obtain expressions for concurrence of the two-qubit subsystems of the N-qubit states under consideration [25] [26]. In this paper, we construct the canonical steering ellipsoids of the N-qubit GHZ and $\mathrm{W}\overline{\mathrm{W}}$ states and analyze the volume monogamy relations satisfied by them.

A flow chart of the paper is given here: In Sec. 2, following a brief overview on Majorana representation [10] [11] [12] [13] of pure permutation symmetric multiqubit states, we obtain the nature of N distinct spinors characterizing GHZ, $\mathrm{W}\overline{\mathrm{W}}$ states and their generalized counterparts. Using these, we show that 3-qubit GHZ and $\mathrm{W}\overline{\mathrm{W}}$ states are interconvertible under local operations on

each qubit. In Sec. 3 we analyze the pairwise entanglement features as well as monogamous nature of N-qubit GHZ and $W\bar{W}$ states. Following a primer on canonical forms of two-qubit subsystems of pure N-qubit state in Sec. 4, we construct the canonical steering ellipsoids of GHZ and $W\bar{W}$ states in Sec. 5. The nature of the volume monogamy relation satisfied by $W\bar{W}$ states is obtained and a comparison with that of GHZ and W-class of states is carried out in Sec. 6. Concluding remarks are given in Sec. 7.

2. Majorana Representation of Pure Symmetric Multiqubit States

A system of N-qubits obeying exchange symmetry gets restricted to a $(N+1)$ dimensional Hilbert space spanned by the basis vectors $\{|N/2, k-N/2\rangle, k=0,1,2,\cdots,N\}$ where,

$$|N/2, k-N/2\rangle = \frac{1}{\sqrt{{}^{N}C_{k}}}\left[\left|\underbrace{0,0,\cdots}_{k \text{ times}},\underbrace{1,1,\cdots}_{N-k \text{ times}}\right\rangle + \text{Permutations}\right] \tag{1}$$

are the $N+1$ Dicke states—expressed in the standard qubit basis $|0\rangle, |1\rangle$.

An arbitrary pure symmetric state,

$$|\Psi_{\text{sym}}\rangle = \sum_{k=0}^{N} d_k |N/2, k-N/2\rangle, \tag{2}$$

is specified by the $(N+1)$ complex coefficients d_k. Eliminating an overall phase and normalizing the state (*i.e.*, $\sum_{k=0}^{N}|d_k|^2 = 1$) implies that N complex parameters are required to completely characterize a pure symmetric state of N qubits.

Alternately, Majorana [10] expressed the pure state $|\Psi_{\text{sym}}\rangle$ as a superposition of *symmetrized* states of N spin-1/2 particles:

$$|\Psi_{\text{sym}}\rangle = \mathcal{N}\sum_{P}\hat{P}\{|\varepsilon_1\varepsilon_2,\cdots,\varepsilon_N\rangle\} \tag{3}$$

where

$$|\varepsilon_s\rangle = \cos(\beta_s/2)e^{-i\alpha_s/2}|0\rangle + \sin(\beta_s/2)e^{i\alpha_s/2}|1\rangle,\ s=1,2,\cdots,N \tag{4}$$

denote spinors constituting the pure symmetric state $|\Psi_{\text{sym}}\rangle$. Here $\hat{P}$ denotes the set of all $N!$ permutations and $\mathcal{N}$ corresponds to an overall normalization factor. The N complex parameters $z_s = \tan\frac{\beta_s}{2}e^{i\alpha_s}$, where (α_s, β_s) correspond to orientations of the spinor $|\varepsilon_s\rangle$ (see Equation (4)), offer an alternate parametrization for the pure symmetric N qubit state $|\Psi_{\text{sym}}\rangle$. The two representations given in Equations (2) and (3) of $|\Psi_{\text{sym}}\rangle$ together lead to the so-called *Majorana polynomial equation*: [13]

$$P(z) = \sum_{k=0}^{N}(-1)^k\sqrt{{}^{N}C_{k}}\,d_k z^k = 0. \tag{5}$$

- The solutions

$$z_s = \tan\frac{\beta_s}{2}e^{i\alpha_s}$$

of the Majorana polynomial Equation (5) determine the orientations (α_s, β_s) of the spinors constituting the state $|\Psi_{\text{sym}}\rangle$, in terms of the collective parameters d_k (see Equation (2)).

• When the Majorana Polynomial $P(z)$ is of degree $r < N$, it is necessary to recast the polynomial $P(z)$ in terms of $z' = \frac{1}{z} = \cot\left(\frac{\beta_s}{2}\right)e^{-i\alpha_s}$ so that the $N-r$ solutions

$$P(z') = \sum_{k=0}^{N} (-1)^{N-k} \sqrt{{}^{N}C_k}\, d_{N-k} z'^{N-k} = 0 \tag{6}$$

of Equation (6) determine the orientations of the remaining $N-r$ spinors constituting the state $|\Psi_{\text{sym}}\rangle$. In other words, given the parameters d_k, the N roots $z_s, s = 1,2,\cdots,N$ of the Majorana polynomials (5), (6) determine the orientations (α_s, β_s) of the spinors constituting the pure symmetric N-qubit state $|\Psi_{\text{sym}}\rangle$.

• When all the spinors in (Equation (3)) are distinct, the family of states is denoted by $\mathcal{D}_{1,1,1,\cdots,1}$ indicating that each of the N-spinors in the N-qubit pure symmetric state appear only once in the symmetrized combination Equation (3). The family of states $\mathcal{D}_{N-k,k}$ denotes the family of states with two distinct spinors one of them repeating k times and the other $N-k$ times in Equation (3), $k = 1,2,3,\cdots,\left[\frac{N}{2}\right]$.

• Dicke states are prominent members of the family $\mathcal{D}_{N-k,k}$. In the following, we show that N-qubit GHZ and $\text{W}\bar{\text{W}}$ states belong to the family $\mathcal{D}_{1,1,1,\cdots,1}$, with N-distinct spinors.

2.1. Majorana Spinors of N-Qubit GHZ and $\text{W}\bar{\text{W}}$ States

Consider the N-qubit GHZ state

$$|\text{GHZ}\rangle_N = \frac{|0_1 0_2 \cdots 0_N\rangle + |1_1 1_2 \cdots 1_N\rangle}{\sqrt{2}}, \tag{7}$$

expressed in terms of the angular momentum states $|jm\rangle$, $j = N/2$, $m = -j$ to j as

$$|\text{GHZ}\rangle_N = \frac{\left|\frac{N}{2},\frac{N}{2}\right\rangle + \left|\frac{N}{2},-\frac{N}{2}\right\rangle}{\sqrt{2}}. \tag{8}$$

Comparing Equation (8) with Equation (3), it can be seen that there are only two non-zero coefficients $d_0 = d_N = 1/\sqrt{2}$. The Majorana polynomial Equation (5) for $|\text{GHZ}\rangle_N$ turns out to be

$$1 + (-1)^N z^N = 0 \tag{9}$$

• Thus the N^{th} roots of unity determine the N-distinct spinors of $|\text{GHZ}\rangle_N$ when N is odd and N^{th} roots of -1 when N is even.

• When $N = 3$, $z_1 = \omega^3 = 1$, $z_2 = \omega^2$, $z_3 = \omega$ where $\omega = \exp i\pi/3$ are the

cube roots of unity and the Majorana spinors

$$|\varepsilon_1\rangle=\frac{1}{\sqrt{2}}\big(|0\rangle+|1\rangle\big),\ |\varepsilon_2\rangle=\frac{1}{\sqrt{2}}\big(|0\rangle+\omega^2|1\rangle\big),\ |\varepsilon_3\rangle=\frac{1}{\sqrt{2}}\big(|0\rangle+\omega|1\rangle\big). \tag{10}$$

constitute $|\mathrm{GHZ}\rangle_3$.

• One may verify explicitly that symmetrization of the spinors (10) leads to the GHZ state:

$$\begin{aligned}|\mathrm{GHZ}\rangle_3=&\frac{1}{\sqrt{6}}\big[|\varepsilon_1,\varepsilon_2,\varepsilon_3\rangle+|\varepsilon_3,\varepsilon_1,\varepsilon_2\rangle+|\varepsilon_2,\varepsilon_3,\varepsilon_1\rangle\\&+|\varepsilon_2,\varepsilon_1,\varepsilon_3\rangle+|\varepsilon_3,\varepsilon_2,\varepsilon_1\rangle+|\varepsilon_1,\varepsilon_3,\varepsilon_2\rangle\big]\\=&\frac{|0_1 0_2 0_3\rangle+|1_1 1_2 1_3\rangle}{\sqrt{2}}\end{aligned} \tag{11}$$

• In a similar manner, the fourth roots of −1 lead to the following spinors corresponding to $|\mathrm{GHZ}\rangle_4$:

$$\begin{aligned}|\varepsilon_1\rangle&=\frac{1}{\sqrt{2}}\big(|0\rangle+\mathrm{e}^{i\pi/4}|1\rangle\big)\\|\varepsilon_2\rangle&=\frac{1}{\sqrt{2}}\big(|0\rangle+\mathrm{e}^{3i\pi/4}|1\rangle\big)\\|\varepsilon_3\rangle&=\frac{1}{\sqrt{2}}\big(|0\rangle+\mathrm{e}^{5i\pi/4}|1\rangle\big)\\|\varepsilon_4\rangle&=\frac{1}{\sqrt{2}}\big(|0\rangle+\mathrm{e}^{7i\pi/4}|1\rangle\big).\end{aligned} \tag{12}$$

The symmetrization of the four spinors (12) as in (3) results in

$$|\mathrm{GHZ}\rangle_4=\mathcal{N}\sum_P\hat{P}\big\{|\varepsilon_1,\varepsilon_2,\varepsilon_3,\varepsilon_4\rangle\big\}=\frac{|0_1 0_2 0_3 0_4\rangle+|1_1 1_2 1_3 1_4\rangle}{\sqrt{2}}, \tag{13}$$

the 4-qubit GHZ state expressed in the qubit basis.

It is evident from the discussion above, that the *N*-qubit GHZ state is a pure symmetric state characterized by *N*-distinct spinors. In the following, we show that the superposition of *N*-qubit W state $|\mathrm{W}\rangle_N$ and its obverse state $|\bar{\mathrm{W}}\rangle_N$ is a pure symmetric state with *N* distinct spinors $|\varepsilon_r'\rangle$, $r=1,2,\cdots,N$.

We first express the *N*-qubit W state $|\mathrm{W}\rangle_N$, its obverse state $|\bar{\mathrm{W}}\rangle_N$ in the angular momentum and qubit basis respectively:

$$|\mathrm{W}\rangle_N=\left|\frac{N}{2},\frac{N}{2}-1\right\rangle=\frac{|1_1 0_2\cdots 0_N\rangle+|0_1 1_2 0_3\cdots 0_N\rangle+\cdots+|0_1 0_2\cdots 1_N\rangle}{\sqrt{N}},$$

$$|\bar{\mathrm{W}}\rangle_N=\left|\frac{N}{2},1-\frac{N}{2}\right\rangle=\frac{|0_1 1_2\cdots 1_N\rangle+|1_1 0_2 1_3\cdots 1_N\rangle+\cdots+|1_1 1_2\cdots 0_N\rangle}{\sqrt{N}},$$

The equal superposition of $|\mathrm{W}\rangle_N$, $|\bar{\mathrm{W}}\rangle_N$, which we refer to as $\mathrm{W}\bar{\mathrm{W}}$ state, is given by

$$|\mathrm{W}\bar{\mathrm{W}}\rangle_N=\frac{\left|\frac{N}{2},\frac{N}{2}-1\right\rangle+\left|\frac{N}{2},1-\frac{N}{2}\right\rangle}{\sqrt{2}} \tag{14}$$

$$= \frac{1}{\sqrt{2}}\left(\left[\frac{|1_1 0_2 \cdots 0_N\rangle + |0_1 1_2 0_3 \cdots 0_N\rangle + \cdots + |0_1 0_2 \cdots 1_N\rangle}{\sqrt{N}}\right] + \left[\frac{|0_1 1_2 \cdots 1_N\rangle + |1_1 0_2 1_3 \cdots 1_N\rangle + \cdots + |1_1 1_2 \cdots 0_N\rangle}{\sqrt{N}}\right]\right). \quad (15)$$

• Comparing Equation (14) with Equation (2), we have $d_1 = d_{N-1} = 1/\sqrt{2}$ as the only non-zero coefficients and hence the corresponding Majorana polynomial Equation (5) turns out to be

$$z + (-1)^N z^{N-1} = 0 \Rightarrow z = 0,\ 1 + (-1)^N z^{N-2} = 0. \quad (16)$$

• The solutions of Equation (16) determine the $N-1$ spinors corresponding to $|W\bar{W}\rangle_N$ and the solution $z' = 1/z = 0$ of the Majorana polynomial Equation (6) determines its N^{th} spinor. Recalling that $z = \tan\frac{\beta}{2}e^{i\alpha}$, $z' = \cot\frac{\beta}{2}e^{-i\alpha}$ we proceed to determine the nature of Majorana spinors (see Equation (4)) constituting $|W\bar{W}\rangle_N$:

$$z_1 = \tan\frac{\beta_1}{2}e^{i\alpha_1} = 0 \Rightarrow \beta_1 = 0,\ \alpha_1 \text{ arbitrary}. \quad (17)$$

Let us choose $\alpha_1 = 0$ to obtain

$$|\varepsilon_1'\rangle = |0\rangle. \quad (18)$$

• The other $N-2$ spinors of the $|W\bar{W}\rangle_N$ state are then given by

$$z^{N-2} = 1 \text{ when } N \text{ is odd} \quad (19)$$

$$z^{N-2} = -1 \text{ when } N \text{ is even} \quad (20)$$

• Note that the N^{th} spinor corresponds to the solution $z_N' = \cot\frac{\beta_N}{2}e^{-i\alpha_N} = 0$ of Equation (6) and we get $\beta_N = \pi$, α_N arbitrary. Choosing $\alpha_N = 0$ we find that

$$|\varepsilon_N'\rangle = |1\rangle. \quad (21)$$

• In adition to the two spinors $|\varepsilon_1'\rangle = |0\rangle$, $|\varepsilon_N'\rangle = |1\rangle$ (which are irrespective of any N) constituting the state $|W\bar{W}\rangle_N$, rest of the distinct spinors are obtained to be the $(N-2)^{\text{th}}$ roots of unity when N is odd and $(N-2)^{\text{th}}$ roots of -1 when N is even [27].

• For $N = 3$, the spinor corresponding to the solution $z = 1 = \tan\frac{\beta_2}{2}e^{i\alpha_2}$ of Equation (19) is characterized by the parameters $\beta_2 = \pi/2$ and $\alpha_2 = 0$. In other words, the *three* distinct spinors $|\varepsilon_r'\rangle$, $r = 1,2,3$ constituting $|W\bar{W}\rangle_3$ are given by

$$|\varepsilon_1'\rangle = |0\rangle, \text{ and } |\varepsilon_2'\rangle = \frac{|0\rangle + i|1\rangle}{\sqrt{2}},\ |\varepsilon_3'\rangle = |1\rangle. \quad (22)$$

• When $N = 4$, the Majorana spinors corresponding to $|W\bar{W}\rangle_4$ are given by

$$\begin{aligned}
|\varepsilon_1'\rangle &= |0\rangle, \\
|\varepsilon_2'\rangle &= \frac{1}{\sqrt{2}}\left(|0\rangle + i|1\rangle\right) \\
|\varepsilon_3'\rangle &= \frac{1}{\sqrt{2}}\left(|0\rangle - i|1\rangle\right) \\
|\varepsilon_4'\rangle &= |1\rangle.
\end{aligned} \tag{23}$$

• One may verify explicitly that

$$\begin{aligned}
\left|\mathrm{W}\bar{\mathrm{W}}\right\rangle_3 &= \frac{1}{\sqrt{6}}\left[|\varepsilon_1', \varepsilon_2', \varepsilon_3'\rangle + |\varepsilon_3', \varepsilon_1', \varepsilon_2'\rangle + |\varepsilon_2', \varepsilon_3', \varepsilon_1'\rangle\right. \\
&\quad \left. + |\varepsilon_2', \varepsilon_1', \varepsilon_3'\rangle + |\varepsilon_3', \varepsilon_2', \varepsilon_1'\rangle + |\varepsilon_1', \varepsilon_3', \varepsilon_2'\rangle\right] \\
&= \frac{|0_1 0_2 1_3\rangle + |0_1 1_2 0_3\rangle + |1_1 0_2 0_3\rangle + |1_1 1_2 0_3\rangle + |1_1 0_2 1_3\rangle + |0_1 1_2 1_3\rangle}{\sqrt{6}}.
\end{aligned} \tag{24}$$

Similarly one may verify explicitly that $\left|\mathrm{W}\bar{\mathrm{W}}\right\rangle_4$ is constructed by symmetrizing the 4 spinors given in Equation (23).

• From the above discussion it is clear that both $\left|\mathrm{GHZ}\right\rangle_N$ and $\left|\mathrm{W}\bar{\mathrm{W}}\right\rangle_N$ belong to the family $\mathcal{D}_{1,1,1,\cdots,1}$ of pure symmetric N-qubit states characterized by N-distinct spinors.

2.2. Majorana Spinors of Generalised N-Qubit GHZ and $\mathrm{W}\bar{\mathrm{W}}$ States

Generalized N-qubit GHZ and $\mathrm{W}\bar{\mathrm{W}}$ states are respectively given by

$$\left|\mathrm{GHZ}\right\rangle_N^{\mathrm{gen}} = \cos\frac{\theta}{2}\left|\frac{N}{2}, \frac{N}{2}\right\rangle + \sin\frac{\theta}{2}\left|\frac{N}{2}, -\frac{N}{2}\right\rangle \tag{25}$$

and

$$\left|\mathrm{W}\bar{\mathrm{W}}\right\rangle_N^{\mathrm{gen}} = \cos\frac{\theta}{2}\left|\frac{N}{2}, \frac{N}{2}-1\right\rangle + \sin\frac{\theta}{2}\left|\frac{N}{2}, 1-\frac{N}{2}\right\rangle. \tag{26}$$

where $\theta \in (0, \pi/4)$.

• From Equations (2), (25), (26), we have $d_0 = \sin(\theta/2)$, $d_N = \cos(\theta/2)$ for $\left|\mathrm{GHZ}\right\rangle_N^{\mathrm{gen}}$; $d_1 = \sin(\theta/2)$ and $d_{N-1} = \cos(\theta/2)$ for $\left|\mathrm{W}\bar{\mathrm{W}}\right\rangle_N^{\mathrm{gen}}$.

• For the 3-qubit state $\left|\mathrm{GHZ}\right\rangle_3^{\mathrm{gen}}$, the Majorana polynomial Equation (5) takes the form

$$\sin\frac{\theta}{2} - z^3\cos\frac{\theta}{2} = 0 \Rightarrow 1 - \left(\frac{z}{\eta}\right)^3 = 0 \quad \text{where } \eta = \left(\tan\frac{\theta}{2}\right)^{\frac{1}{3}}$$

leading to the roots

$$z_1 = \eta\omega^3 = \eta, \; z_2 = \eta\omega^2, \; z_3 = \eta\omega \tag{27}$$

$\omega, \omega^2, \omega^3 = 1$ are the cube roots of unity.

• The three Majorana spinors corresponding to $\left|\mathrm{GHZ}\right\rangle_3^{\mathrm{gen}}$ (see Equation (25)) are therefore given by

$$|\varepsilon_1\rangle^{\mathrm{gen}} = \frac{1}{\sqrt{1+\eta^2}}\begin{pmatrix}1\\ \eta\end{pmatrix}, \; |\varepsilon_2\rangle^{\mathrm{gen}} = \frac{1}{\sqrt{1+\eta^2}}\begin{pmatrix}1\\ \eta\omega\end{pmatrix}, |\varepsilon_3\rangle^{\mathrm{gen}} = \frac{1}{\sqrt{1+\eta^2}}\begin{pmatrix}1\\ \eta\omega^2\end{pmatrix}. \tag{28}$$

- With $d_1 = \sin(\theta/2)$ and $d_2 = \cos(\theta/2)$ for $\left|\mathrm{W}\bar{\mathrm{W}}\right\rangle_3^{\mathrm{gen}}$, the independent roots of Majorana polynomial equation (see Equation (5)) $z\sin\frac{\theta}{2} - z^2\cos\frac{\theta}{2} = 0$ and (see Equation (6)) $z'^2\cos\frac{\theta}{2} - z'\sin\frac{\theta}{2} = 0$, $z' = 1/z$ are

$$z_1 = 0,\ z_2 = \tan\frac{\theta}{2} = \eta^3,\ z_3 = \frac{1}{z} = 0. \tag{29}$$

- Thus the Majorana spinors of $\left|\mathrm{W}\bar{\mathrm{W}}\right\rangle_3^{\mathrm{gen}}$ turn out be

$$\left|\varepsilon_1'\right\rangle^{\mathrm{gen}} = \begin{pmatrix}1\\0\end{pmatrix},\ \left|\varepsilon_2'\right\rangle^{\mathrm{gen}} = \frac{1}{\sqrt{1+\eta^6}}\begin{pmatrix}1\\\eta^3\end{pmatrix},\ \left|\varepsilon_3'\right\rangle^{\mathrm{gen}} = \begin{pmatrix}0\\1\end{pmatrix}. \tag{30}$$

- In general, the N spinors corresponding to $\left|\mathrm{GHZ}\right\rangle_N^{\mathrm{gen}}$ are given by

$$\left|\varepsilon_k\right\rangle = \frac{1}{\sqrt{1+\chi^2}}\begin{pmatrix}1\\ \chi \mathrm{e}^{i\left(\frac{\phi+2k\pi}{N}\right)}\end{pmatrix},\ k = 0,1,2,\cdots,N-1,\ \chi = \left(\tan\frac{\theta}{2}\right)^{\frac{1}{N}} \tag{31}$$

- Note that $\phi = 0$ when N is odd and $\phi = \pi$ when N is even.
- Similarly the N spinors corresponding to $\left|\mathrm{W}\bar{\mathrm{W}}\right\rangle_N^{\mathrm{gen}}$ are,

$$\left|\varepsilon_1'\right\rangle = \begin{pmatrix}1\\0\end{pmatrix},$$

$$\left|\varepsilon_2'\right\rangle = \frac{1}{\sqrt{1+\xi^2}}\begin{pmatrix}1\\ \xi \mathrm{e}^{i\left(\frac{\phi+2k'\pi}{N-2}\right)}\end{pmatrix},\ k' = 0,1,\cdots,N-3 \text{ and } \xi = \left(\tan\frac{\theta}{2}\right)^{\frac{1}{N-2}} \tag{32}$$

$$\left|\varepsilon_3'\right\rangle = \begin{pmatrix}0\\1\end{pmatrix},$$

Here too, $\phi = 0$ when $N-2$ is odd and $\phi = \pi$ when $N-2$ is even.

2.3. Interconvertibility of 3-Qubit GHZ and $\mathrm{W}\bar{\mathrm{W}}$ States under Local Operations

If the states (11), (24) are related to each other by identical local operations of the form $A\otimes A\otimes A$, *i.e.*,

$$\left|\mathrm{GHZ}\right\rangle_3 = \mathcal{N}\left(A\otimes A\otimes A\right)\left|\mathrm{W}\bar{\mathrm{W}}\right\rangle_3 \tag{33}$$

the corresponding Majorana spinors (10) and (22) must be related to each other through $\left|\varepsilon_r\right\rangle \propto A\left|\varepsilon_s'\right\rangle$, $r,s = 1,2,3$; N is the normalization constant. We consider an arbitrary 2×2 invertible matrix $A = \begin{pmatrix}a & b\\ c & d\end{pmatrix}$, $\det A = ad - bc = 1$ and explicitly solve the following equations relating Majorana spinors (10) and (22):

$$\begin{aligned}
&\left|\varepsilon_1\right\rangle = N_1 A\left|\varepsilon_1'\right\rangle \Rightarrow \frac{1}{\sqrt{2}}\begin{pmatrix}1\\1\end{pmatrix} = N_1\begin{pmatrix}a & b\\ c & d\end{pmatrix}\begin{pmatrix}1\\0\end{pmatrix}\\
&\left|\varepsilon_2\right\rangle = N_2 A\left|\varepsilon_2'\right\rangle \Rightarrow \frac{1}{\sqrt{2}}\begin{pmatrix}1\\\omega^2\end{pmatrix} = N_2\begin{pmatrix}a & b\\ c & d\end{pmatrix}\frac{1}{\sqrt{2}}\begin{pmatrix}1\\1\end{pmatrix}\\
&\left|\varepsilon_3\right\rangle = N_3 A\left|\varepsilon_3'\right\rangle \Rightarrow \frac{1}{\sqrt{2}}\begin{pmatrix}1\\\omega\end{pmatrix} = N_3\begin{pmatrix}a & b\\ c & d\end{pmatrix}\begin{pmatrix}0\\1\end{pmatrix}
\end{aligned} \tag{34}$$

It can be seen that the SL (2, C) matrix

$$A=\frac{1}{\omega(\omega-1)}\begin{pmatrix}1 & \omega\\ 1 & \omega^2\end{pmatrix}, \tag{35}$$

and the proportionality constants

$$N_1=\sqrt{2},\ N_2=-\omega^2,\ N_3=\omega\sqrt{2} \tag{36}$$

lead to the transformation (33). In other words, the 3-qubit $\mathrm{W}\bar{\mathrm{W}}$ state (24) gets transformed to the 3-qubit GHZ state (11) under identical local operations (35) on all the three qubits.

3. Pairwise Entanglement Features of *N*-Qubit $\mathrm{W}\bar{\mathrm{W}}$ States

We adopt concurrence [28] [29] to quantify the pairwise entanglement in $\mathrm{W}\bar{\mathrm{W}}$ states. The concurrence $C(\rho)$ of any two-qubit state ρ is defined as [28] [29]

$$C(\rho)=\max\left(0,\sqrt{\lambda_1}-\sqrt{\lambda_2}-\sqrt{\lambda_3}-\sqrt{\lambda_4}\right) \tag{37}$$

where λ_i, $i=1,2,3,4$ are the eigenvalues of the 4 × 4 matrix $R=\rho\left(\sigma_y\otimes\sigma_y\right)\rho^*\left(\sigma_y\otimes\sigma_y\right)$ arranged in the decreasing order $\lambda_1\geq\lambda_2\geq\lambda_3\geq\lambda_4$.

In order to evaluate the pairwise entanglement features of *N*-qubit $\mathrm{W}\bar{\mathrm{W}}$ states, we need to evaluate the structure of its two-qubit subsystems. The state $\left|\mathrm{W}\bar{\mathrm{W}}\right\rangle_N$ being a symmetric state, its two qubit reduced density matrices are all identical and from its structure in the qubit basis (see Equation (15)) one can readily evaluate the two-qubit reduced density matrices $\rho_2^{(N)}=\mathrm{Tr}_{N-2}\left|\mathrm{W}\bar{\mathrm{W}}\right\rangle_N\left\langle\mathrm{W}\bar{\mathrm{W}}\right|$. We denote $R_N=\rho_2^{(N)}\left(\sigma_y\otimes\sigma_y\right)\rho_2^{(N)*}\left(\sigma_y\otimes\sigma_y\right)$ associated with the reduced two-qubit system $\rho_2^{(N)}$ of the *N*-qubit state $\left|\mathrm{W}\bar{\mathrm{W}}\right\rangle_N$.

• For the state $\left|\mathrm{W}\bar{\mathrm{W}}\right\rangle_3$ (see Equation (24)), the two qubit reduced density matrix obtained by tracing out *any* one qubit is given by

$$\begin{aligned}\rho_2^{(3)}=\frac{1}{6}\big[&|00\rangle\langle 00|+|00\rangle\langle 01|+|00\rangle\langle 10|+|01\rangle\langle 00|+2|01\rangle\langle 01|+2|01\rangle\langle 10|\\&+|01\rangle\langle 11|+|10\rangle\langle 00|+2|10\rangle\langle 01|+2|10\rangle\langle 10|+|10\rangle\langle 11|+|11\rangle\langle 01|\\&+|11\rangle\langle 10|+|11\rangle\langle 11|\big].\end{aligned} \tag{38}$$

On expressing $\rho_2^{(3)}$ in 4 × 4 matrix form (in the basis $\{|00\rangle,|01\rangle,|10\rangle,|11\rangle\}$, we have

$$\rho_2^{(3)}=\frac{1}{6}\begin{pmatrix}1 & 1 & 1 & 0\\ 1 & 2 & 2 & 1\\ 1 & 2 & 2 & 1\\ 0 & 1 & 1 & 1\end{pmatrix}. \tag{39}$$

• For the 4 qubit $\mathrm{W}\bar{\mathrm{W}}$ state

$$\begin{aligned}\left|\mathrm{W}\bar{\mathrm{W}}\right\rangle_4=\frac{1}{4}\big[&|1_1 0_2 0_3 0_4\rangle+|0_1 1_2 0_3 0_4\rangle+|0_1 0_2 1_3 0_4\rangle+|0_1 0_2 0_3 1_4\rangle\\&+|0_1 1_2 1_3 1_4\rangle+|1_1 0_2 1_3 1_4\rangle+|1_1 1_2 0_3 1_4\rangle+|1_1 1_2 1_3 0_4\rangle\big],\end{aligned}$$

the two-qubit reduced density matrix $\rho_2^{(4)}$, obtained by tracing over any

two-qubits of $\left|W\bar{W}\right\rangle_4$, is given by

$$\rho_2^{(4)} = \frac{1}{4}\Big[|00\rangle\langle 00| + |00\rangle\langle 11| + |01\rangle\langle 01| + |01\rangle\langle 10| + |10\rangle\langle 01| + |10\rangle\langle 10| + |11\rangle\langle 00| + |11\rangle\langle 11|\Big]. \tag{40}$$

Thus, the 4×4 matrix representation of $\rho_2^{(4)}$ in the standard two-qubit basis is

$$\rho_2^{(4)} = \frac{1}{4}\begin{pmatrix} 1 & 0 & 0 & 1 \\ 0 & 1 & 1 & 0 \\ 0 & 1 & 1 & 0 \\ 1 & 0 & 0 & 1 \end{pmatrix}. \tag{41}$$

• For any $N > 4$, tracing out $(N-2)$ qubits of $\left|W\bar{W}\right\rangle_N$ (see Equation (15)) leads to the two qubit reduced density matrix $\rho_2^{(N)}$:

$$\begin{aligned} \rho_2^{(N)} &= \frac{N-2}{2N}\Big[|00\rangle\langle 00| + |11\rangle\langle 11|\Big] \\ &\quad + \frac{1}{N}\Big[|01\rangle\langle 01| + |01\rangle\langle 10| + |10\rangle\langle 01| + |10\rangle\langle 10|\Big] \\ &= \begin{pmatrix} \frac{N-2}{2N} & 0 & 0 & 0 \\ 0 & \frac{1}{N} & \frac{1}{N} & 0 \\ 0 & \frac{1}{N} & \frac{1}{N} & 0 \\ 0 & 0 & 0 & \frac{N-2}{2N} \end{pmatrix}. \end{aligned} \tag{42}$$

• On explicit evaluation of the eigenvalues of $R_3 = \rho_2^{(3)}\left(\sigma_y \otimes \sigma_y\right)\rho_2^{(3)*}$, we find that $\lambda_1 = 1/4$, $\lambda_2 = 1/36$, $\lambda_3 = \lambda_4 = 0$ for $N = 3$. Thus, the concurrence of the state $\rho_2^{(3)}$ is $C^{(3)} = 1/3$. For $N = 4$, the matrix R_N has only two non-zero eigenvalues $\lambda_1 = \lambda_2 = 1/4$, implying that the concurrence of the two-qubit reduced system $\rho_2^{(4)}$ of $\left|W\bar{W}\right\rangle_4$ state is zero.

• For any $N > 4$, the eigenvalues of $R_N = \rho_2^{(N)}\left(\sigma_y \otimes \sigma_y\right)\rho_2^{(N)*}\left(\sigma_y \otimes \sigma_y\right)$ are

$$\lambda_1 = \lambda_2 = \frac{N-2}{2N}, \quad \lambda_3 = \frac{2}{N}, \quad \lambda_4 = 0. \tag{43}$$

• For $N = 5, 6$, the values of λ_i, $i = 1, 2, 3, 4$ are found to be

$$\begin{aligned} N = 5 &: \lambda_1 = \lambda_2 = \frac{3}{10}, \lambda_3 = \frac{2}{5}, \lambda_4 = 0 \\ N = 6 &: \lambda_1 = \lambda_2 = \frac{1}{3}, \lambda_3 = \frac{2}{3}, \lambda_4 = 0. \end{aligned} \tag{44}$$

• It can be seen from Equation (44) that $\sqrt{\lambda_1} - \sqrt{\lambda_2} - \sqrt{\lambda_3} - \sqrt{\lambda_4}$ turns out to be negative and hence concurrence (see Equation (37)) of the $W\bar{W}$ state vanishes when $N = 5, 6$.

• From Equation (43), we have $\lambda_{1,2} > \lambda_3$ when $N > 6$. The highest eigenvalue $\lambda_1 = \lambda_2$ being doubly repeated, concurrence of the state $\left|W\bar{W}\right\rangle_N$ vanishes for $N > 6$. In other words, except for the reduced two-qubit systems $\rho_2^{(3)}$ of

the the 3-qubit state $\left|\mathrm{W}\bar{\mathrm{W}}\right\rangle_3$, the concurrence for $\rho_2^{(N)}$ drawn from $\left|\mathrm{W}\bar{\mathrm{W}}\right\rangle_N$ vanishes when $N>3$. Thus, there is no pairwise entanglement in $\left|\mathrm{W}\bar{\mathrm{W}}\right\rangle_N$ state except when $N=3$.

It is well-known that there is a trade-off between entanglement shared by multiple parties. We explore these restrictions on shareability or monogamy of entanglement in *N*-qubit $\mathrm{W}\bar{\mathrm{W}}$ states. The Coffman-Kundu-Wootters inequality for monogamy of concurrence in a pure three-qubit state is given by [21]

$$C_{12}^2+C_{13}^2\le C_{1(23)}^2 \tag{45}$$

where C_{12}, C_{13} denote concurrences of two-qubit reduced systems 1,2 and 1,3 respectively; $C_{1(23)}$ is the concurrence of the bipartition 1-23. The 3-tangle of a three-qubit state τ_3, defined by [21]

$$\tau_3=C_{1(23)}^2-C_{12}^2-C_{13}^2 \tag{46}$$

is a measure of *residual entanglement* [30], which is not accounted by the entanglement between two-qubit subsystems of a three-qubit pure state. The 3-tangle $\tau_3=1$ for three-qubit GHZ states and $\tau_3=0$ for W states.

A generalization of the 3-tangle to any *N*-qubit pure states, called *N*-tangle, has also been proposed [31] [32]. The *N*-tangle τ_N for a pure symmetric *N*-qubit state $\left|\Psi\right\rangle_{\mathrm{sym}}$ is given by

$$\tau_N=4\det\rho_1^{(N)}-(N-1)C^2;\ \ \rho_1^N=\mathrm{Tr}_{N-1}\left|\Psi\right\rangle_{\mathrm{sym}}\left\langle\Psi\right|. \tag{47}$$

• One can readily see, by tracing out a qubit from the two-qubit density matrices (39), (41)), that the single qubit density matrices $\rho_1^{(3)}$, $\rho_1^{(4)}$ of $\left|\mathrm{W}\bar{\mathrm{W}}\right\rangle_3$, $\left|\mathrm{W}\bar{\mathrm{W}}\right\rangle_4$ are obtained as,

$$\rho_1^{(3)}=\begin{pmatrix}\frac{1}{2} & \frac{1}{3}\\ \frac{1}{3} & \frac{1}{2}\end{pmatrix} \tag{48}$$

$$\rho_1^{(4)}=\frac{1}{2}\begin{pmatrix}1 & 0\\ 0 & 1\end{pmatrix} \tag{49}$$

• Also, by tracing out a single qubit from the two-qubit states $\rho_2^{(N)}$ (see Equation (42)), it can be readily seen that the single qubit density matrix $\rho_1^{(N)}$ of the state $\left|\mathrm{W}\bar{\mathrm{W}}\right\rangle_N$ turns out to be $I_2/2$ for any $N\ge 4$, where I_2 is the 2×2 identity matrix.

• For the 3-qubit $\mathrm{W}\bar{\mathrm{W}}$ state, we have concurrence $C=1/3$ and $\det\rho_1^{(3)}=5/36$ (see Equation (48)). The 3-tangle $\tau_3=4\det\rho_1^{(3)}-2C^2=1/3$.

• The concurrence *C* between any pair of qubits in $\left|\mathrm{W}\bar{\mathrm{W}}\right\rangle_N$ being zero and $\det\rho_1^{(N)}=\det I_2/2=1/4$, $N\ge 4$, we obtain the *N*-tangle (see Equation (47)) $\tau_N=1$ for $N\ge 4$.

From the above results, we conclude that two-qubit entanglement in *N*-qubit $\mathrm{W}\bar{\mathrm{W}}$ states with $N\ge 4$ vanishes—but their residual entanglement quantified by *N*-tangle τ_N is maximum. The three-qubit $\mathrm{W}\bar{\mathrm{W}}$ state possesses both two-qubit entanglement (quantified by concurrence $C=1/3$) and residual 3-way

entanglement (characterized by $\tau_3^{W\bar{W}} = 1/3$).

It is important to notice that N-qubit GHZ state also has vanishing concurrence and maximum concurrence tangle [21] $\tau = 1$ for any $N \geq 3$. The identical pairwise entanglement and monogamy features of GHZ and $W\bar{W}$ states for any $N \geq 4$ is worth noticing. We examine this aspect with the help of canonical steering ellipsoids in Sec. 5.

4. Canonical Steering Ellipsoids as Geometric Representation of Two-Qubit States

It has been shown [24] [25] [26] that the SLOCC transformation on a two-qubit state is equivalent to the Lorentz congruent transformation (up to a scalar factor) on the real representative of the state. This helps in obtaining the Lorentz canonical form of the real representative of the state and thereby its geometric representation in terms of canonical steering ellipsoiods [24] [25] [26]. While the canonical steering ellipsoids corresponding to two SLOCC inequivalent families of 3-qubit states are obtained in [25], the canonical steering ellipsoids associated with SLOCC inequivalent families of N-qubit Dicke class of states are analysed in [26]. In the following, after a brief description of the concepts used in [24] [25] [26], we proceed to work on the geometrical representation of N-qubit GHZ and $W\bar{W}$ states.

4.1. Real Representation of Two-Qubit States and Their Lorentz Canonical Forms

Consider a two-qubit density matrix ρ_2 expressed in the Hilbert-Schmidt basis $\{\sigma_\mu \otimes \sigma_\nu\}$:

$$\rho_2 = \frac{1}{4}\sum_{\mu,\nu=0}^{3} \Lambda_{\mu\nu}\left(\sigma_\mu \otimes \sigma_\nu\right), \tag{50}$$

The coefficients of expansion $\Lambda_{\mu\nu}$

$$\Lambda_{\mu\nu} = \mathrm{Tr}\left[\rho_2\left(\sigma_\mu \otimes \sigma_\nu\right)\right], \tag{51}$$

form a real 4×4 matrix Λ representing the density matrix ρ_2. Here, σ_i, $i = 1,2,3$ are the Pauli spin matrices and σ_0 is the 2×2 identity matrix.

• When the qubits are subjected to local operations on their respective parts, the two-qubit density matrix ρ_2 transforms to $\tilde{\rho}_2$ as

$$\rho_2 \to \tilde{\rho}_2 = \frac{\left(A \otimes B\right)\rho_2\left(A^\dagger \otimes B^\dagger\right)}{\mathrm{Tr}\left[\rho_2\left(A^\dagger A \otimes B^\dagger B\right)\right]}. \tag{52}$$

Here, $A, B \in SL(2,C)$ denote 2×2 complex matrices with unit determinant and represent local operations on the qubits A, B. One can choose suitable local operations A and B such that the two-qubit density matrix ρ_2 attains its canonical form $\tilde{\rho}_2$.

• When the two-qubit state ρ_2 undergoes the transfomation (52), its real representative Λ transforms as [24] [25]

$$\Lambda \to \tilde{\Lambda} = \frac{L_A \Lambda L_B^{\mathrm{T}}}{\left(L_A \Lambda L_B^{\mathrm{T}}\right)_{00}}. \tag{53}$$

Here $L_A, L_B \in SO(3,1)$ are 4 × 4 proper orthochronous Lorentz transformation matrices [33] corresponding respectively to $A, B \in SL(2,C)$ and the superscript "T" denotes transpose operation.

• The Lorentz canonical form [24] $\tilde{\Lambda}$ can be obtained by constructing the 4 × 4 real symmetric matrix $\Omega = \Lambda G \Lambda^{\mathrm{T}}$, where $G = \mathrm{diag}(1,-1,-1,-1)$ denotes the Lorentz metric [33].

• Using the defining property [33] $L^{\mathrm{T}} G L = G$ of Lorentz transformation L, it can be seen that the matrix $G\Omega$ undergoes a *s*imilarity transformation $G\tilde{\Omega} = L^{-1}(G\Omega)L$.

• It has been shown [24] [25] [26] that the canonical form of Λ can either be a diagonal matrix or a non-diagonal matrix with only one off-diagonal element [22] [24] [25] [26] depending on the eigenvalues and eigenvectors of $G\Omega$.

• When the eigenvector X_0 associated with the highest eigenvalue λ_0 of $G\Omega$ obeys the Lorentz invariant condition $X_0^{\mathrm{T}} G X_0 > 0$, Λ assumes the diagonal canonical form $\tilde{\Lambda}_{\mathrm{I}}$ given by

$$\tilde{\Lambda}_{\mathrm{I}} = \mathrm{diag}\left(1, \sqrt{\frac{\lambda_1}{\lambda_0}}, \sqrt{\frac{\lambda_2}{\lambda_0}}, \pm\sqrt{\frac{\lambda_3}{\lambda_0}}\right), \tag{54}$$

where $\lambda_0 \geq \lambda_1 \geq \lambda_2 \geq \lambda_3 > 0$ are the *non-negative* eigenvalues of $G\Omega$.

• Suppose that the non-negative eigenvalues λ_0 and λ_1 ($\lambda_0 \geq \lambda_1$) of $G\Omega$ are doubly degenerate and an eigenvector X_0 of $G\Omega$, belonging to the highest eigenvalue λ_0, satisfies the Lorentz invariant condition $X_0^{\mathrm{T}} G X_0 = 0$. In such cases, the Lorentz canonical form of Λ turns out to be a non-diagonal matrix (with only one non-diagonal element):

$$\tilde{\Lambda}_{\mathrm{II}} = \begin{pmatrix} 1 & 0 & 0 & 0 \\ 0 & a_1 & 0 & 0 \\ 0 & 0 & -a_1 & 0 \\ 1-a_0 & 0 & 0 & a_0 \end{pmatrix} \tag{55}$$

The parameters a_0, a_1 in Equation (55) are given by [24] [25] [26]

$$a_0 = \frac{\lambda_0}{\phi_0}, \; a_1 = \sqrt{\frac{\lambda_1}{\phi_0}} \tag{56}$$

where ϕ_0 is the 00$^{\mathrm{th}}$ element of the canonical form $\tilde{\Omega}_{\mathrm{II}} = \tilde{\Lambda}_{\mathrm{II}} G \tilde{\Lambda}_{\mathrm{II}}^{\mathrm{T}}$:

$$\tilde{\Omega}_{\mathrm{II}} = \begin{pmatrix} \phi_0 & 0 & 0 & \phi_0 - \lambda_0 \\ 0 & -\lambda_1 & 0 & 0 \\ 0 & 0 & -\lambda_1 & 0 \\ \phi_0 - \lambda_0 & 0 & 0 & \phi_0 - 2\lambda_0 \end{pmatrix}. \tag{57}$$

4.2. Steering Ellipsoids Corresponding to Lorentz Canonical Form of Two-Qubit States

In the two-qubit state ρ_2, local projective valued measurements (PVM)

$$Q = I_2 + \sigma_1 q_1 + \sigma_2 q_2 + \sigma_3 q_3,\ \ q_1^2 + q_2^2 + q_3^2 = 1 \tag{58}$$

on Bob's qubit leads to collapsed states of Alice's qubit characterized by Bloch vectors $\mathbf{p}_A = (p_1, p_2, p_3)^{\mathrm{T}}$ through the transformation [24]

$$(1, p_1, p_2, p_3)^{\mathrm{T}} = \Lambda (1, q_1, q_2, q_3)^{\mathrm{T}},\ \ q_1^2 + q_2^2 + q_3^2 = 1. \tag{59}$$

Here $\mathbf{q}_B = (q_1, q_2, q_3)^{\mathrm{T}}$, $q_1^2 + q_2^2 + q_3^2 = 1$ represents points on the Bloch sphere representing all possible PVMs at Bob's end. The steered Bloch vectors $\mathbf{p}_A$ of Alice's qubit constitute an ellipsoidal surface $\mathcal{E}_{A|B}$, enclosed within the Bloch sphere.

• For the diagonal canonical form $\tilde{\Lambda}_{\mathrm{I}}$ (see Equation (54)) of the two-qubit state, it follows from Equation (59) that

$$p_1 = \sqrt{\frac{\lambda_1}{\lambda_0}} q_1,\ \ p_2 = \sqrt{\frac{\lambda_2}{\lambda_0}} q_2,\ \ p_3 = \pm \sqrt{\frac{\lambda_3}{\lambda_0}} q_3, \tag{60}$$

are steered Bloch points $\mathbf{p}_A$ of Alice's qubit. They obey the equation

$$\frac{\lambda_0 p_1^2}{\lambda_1} + \frac{\lambda_0 p_2^2}{\lambda_2} + \frac{\lambda_0 p_3^2}{\lambda_3} = 1 \tag{61}$$

of an ellipsoid with semiaxes $a_1 = \sqrt{\lambda_1/\lambda_0}$, $a_2 = \sqrt{\lambda_2/\lambda_0}$, $a_3 = \sqrt{\lambda_3/\lambda_0}$) and center $(0,0,0)$ inside the Bloch sphere $q_1^2 + q_2^2 + q_3^2 = 1$. We refer to this as the *canonical steering ellipsoid* representing the set of all two-qubit density matrices which are SLOCC equivalent to the canonical form $\tilde{\rho}_{\mathrm{I}}$ (see Equation (52)) corresponding to $\tilde{\Lambda}_{\mathrm{I}}$.

• For the non-diagonal canonical form $\tilde{\Lambda}_{\mathrm{II}}$ (see Equation (55)), we get the coordinates of steered Alice's Bloch vector $\mathbf{p}_A$, on using Equation (59);

$$p_1 = a_1 q_1,\ \ p_2 = -a_1 q_2,\ \ p_3 = (1 - a_0) + a_0 q_3,\ \ q_1^2 + q_2^2 + q_3^2 = 1 \tag{62}$$

and they satisfy the equation

$$\frac{p_1^2}{a_1^2} + \frac{p_2^2}{a_1^2} + \frac{\left(p_3 - (1 - a_0)\right)^2}{a_0^2} = 1. \tag{63}$$

Note that Equation (63) represents the canonical steering spheroid (traced by Alice's Bloch vector $\mathbf{p}_A$) inside the Bloch sphere with its center at $(0,0,1-a_0)$ and lengths of the semiaxes given by $a_0 = \lambda_0/\phi_0$, $a_1 = \sqrt{\lambda_1/\phi_0}$. In other words, a shifted spheroid inscribed within the Bloch sphere, represents two-qubit states that possess a non-diagonal Lorentz canonical form $\tilde{\Lambda}_{\mathrm{II}}$ (see Equation (55)).

In the following, we obtain the Lorentz canonical forms of the real representation $\Lambda^{(N)}$ associated with the two-qubit subsystems $\rho_2^{(N)}$ of N-qubit $\mathrm{W}\bar{\mathrm{W}}$ states for all N and arrive at their canonical steering ellipsoids.

5. Canonical Steering Ellipsoids Corresponding to $\left|\mathrm{W}\bar{\mathrm{W}}\right\rangle_N$

In Sec. 2, we have seen that the N-qubit $\mathrm{W}\bar{\mathrm{W}}$ ($N > 3$) states do not have pairwise entanglement (zero concurrence) and exhibit maximum restriction in the shareability of entanglement among its subsystems (concurrence tangle $\tau = 1$).

In contrast to this, the 3-qubit $W\bar{W}$ state have non-zero concurrence ($C=1/3$) and the concurrence tangle is not maximum ($\tau=1/3$). In this section, we explore how the geometric picture of the two-qubit subsystems of the states $\left|W\bar{W}\right\rangle_N$ reflect this aspect.

5.1. Canonical Steering Ellipsoids Corresponding to $\left|W\bar{W}\right\rangle_3$

The real matrix representation Λ_3 of the two-qubit subsystem $\rho^{(3)}$ (see Equation (39)) of $\left|W\bar{W}\right\rangle_3$ and the real symmetric matrix $\Omega^{(3)}=\Lambda_3 G\left(\Lambda_3\right)^{\mathrm{T}}$ are respectively given by

$$\Lambda_3=\begin{pmatrix} 1 & \frac{2}{3} & 0 & 0 \\ \frac{2}{3} & \frac{2}{3} & 0 & 0 \\ 0 & 0 & \frac{2}{3} & 0 \\ 0 & 0 & 0 & \frac{1}{3} \end{pmatrix} \text{ and } \Omega^{(3)}=\frac{1}{9}\begin{pmatrix} 5 & 2 & 0 & 0 \\ -2 & 0 & 0 & 0 \\ 0 & 0 & 4 & 0 \\ 0 & 0 & 0 & 1 \end{pmatrix}. \tag{64}$$

The normalized eigenvectors X_k of $G\Omega^{(3)}$ belonging to its eigenvalues $\lambda_1=\lambda_2=4/9$, $\lambda_3=\lambda_4=1/9$ can be determined by solving the eigenvalue equation $\left(G\Omega^{(3)}\right)X_k=\lambda_k X_k$, $k=0,1,2,3$. On explicit determination, we get

$$\begin{aligned} X_0&=\frac{2}{\sqrt{3}}(2,-1,0,0)\in\lambda_0=4/9 \\ X_1&=(0,1,0,0)\in\lambda_1=4/9 \\ X_2&=\frac{1}{\sqrt{3}}(1,-2,0,0)\in\lambda_2=1/9 \\ X_3&=(0,0,0,1)\in\lambda_3=1/9 \end{aligned} \tag{65}$$

It can be readily verified that $X_r^{\mathrm{T}}GX_s=g_{rs}$ where $g_{00}=1$, $g_{11}=g_{22}=g_{33}=-1$, $g_{rs}=0$ when $r\neq s$, $r,s=0,1,2,3$ *i.e.*, $X_0^{\mathrm{T}}GX_0=1$ and $X_k^{\mathrm{T}}GX_k=-1$ when $k=1,2,3$. Thus, the set $\{X_0,X_1,X_2,X_3\}$ forms an orthonormal tetrad of Minkowski four-vectors [33]. The 4 × 4 real matrix $L=(X_0,X_1,X_2,X_3)$, constructed using the eigenvectors of $G\Omega^{(3)}$ is a Lorentz matrix [33] satisfying the relation $L^{\mathrm{T}}GL=G$ and $\det L=1$. Explicitly, we have

$$L=\frac{1}{\sqrt{3}}\begin{pmatrix} 2 & -1 & 0 & 0 \\ 0 & 1 & 0 & 0 \\ -1 & 2 & 0 & 0 \\ 0 & 0 & 0 & 1 \end{pmatrix}. \tag{66}$$

From the relations $\left(G\Omega^{(3)}\right)X_k=\lambda_k X_k$, $X_r^{\mathrm{T}}GX_s=g_{rs}$, one can readily see that $\tilde{\Lambda}_3=L\Lambda_3 L^{\mathrm{T}}$ is a diagonal matrix with elements $a_k=\sqrt{\frac{\lambda_k}{\lambda_0}}$. With $\lambda_1=\lambda_2=4/9$, $\lambda_3=\lambda_4=1/9$, we have $a_1=1$, $a_2=a_3=1/2$.

From the discussion in Sec. 4.2 leading to Equation (61), it can be seen that

the canonical steering ellipsoid corresponding to $\left|\mathrm{W}\overline{\mathrm{W}}\right\rangle_3$ is an oblate spheroid with radius 1/2 centered at the origin and touching the Bloch sphere (see Figure 1).

5.2. Geometrical Representation of 4-Qubit $\mathrm{W}\overline{\mathrm{W}}$ States

The two-qubit subsystem $\rho_2^{(4)}$ of the 4-qubit $\mathrm{W}\overline{\mathrm{W}}$ state given in Equation (41) leads to the diagonal structure of its real representative Λ_4;

$$\Lambda_4 = \mathrm{diag}(1,1,0,0) \tag{67}$$

Thus $G\Omega^{(4)} = G\left(\Lambda_4 G\left(\Lambda_4\right)^{\mathrm{T}}\right) = \Lambda_4$ and it is already in its canonical form. The eigenvector belonging to the largest eigenvalue $\lambda_0 = \lambda_1 = 1$ is $X_0 = (1,0,0,0)$ of $G\Omega^{(4)}$ and satisfies the relation $\left(X_0\right)^{\mathrm{T}} G X_0 = 1$. With the other two eigenvalues of $G\Omega^{(4)}$ being $\lambda_2 = \lambda_3 = 0$, the parameters $a_1 = \sqrt{\lambda_1/\lambda_0}$, $a_2 = a_3 = \sqrt{\lambda_{2,3}/\lambda_0}$ are $a_1 = 1$, $a_2 = a_3 = 0$ *i.e.*, the tip of Bloch vectors of one qubit, steered by another qubit of the 4-qubit $\mathrm{W}\overline{\mathrm{W}}$ state trace a straight line joining the north and south poles of the Bloch sphere.

It is of interest to note here that the *N*-qubit GHZ states have the same geometrical representation as that of 4 qubit $\mathrm{W}\overline{\mathrm{W}}$ states. More specifically, the two-qubit subsystem density matrix of $\left|\mathrm{GHZ}\right\rangle_N$ is given by $\rho_2^{\mathrm{GHZ}} = \mathrm{diag}(1/2,0,0,1/2)$ and its real representative is found to be

$$\Lambda_N^{\mathrm{GHZ}} = diag\,(1,0,0,1). \tag{68}$$

It readily follows that $G\Omega_{\mathrm{GHZ}}^{(N)} = G\left(\Lambda_N^{\mathrm{GHZ}} G\left(\Lambda_N^{\mathrm{GHZ}}\right)^{\mathrm{T}}\right) = \Lambda_N^{\mathrm{GHZ}}$. The eigenstructures of $G\Omega$ corresponding to *N*-qubit GHZ states and 4-qubit $\mathrm{W}\overline{\mathrm{W}}$ state are identical. The two-qubit subsystem density matrix of *N*-qubit GHZ state is represented by a straight line joining north and south poles of the Bloch sphere.

5.3. Canonical Steering Ellipsoids Corresponding to *N*-Qubit $\mathrm{W}\overline{\mathrm{W}}$ States; $N > 4$

In order to obtain the geometrical representation of *N*-qubit $\mathrm{W}\overline{\mathrm{W}}$ states for $N > 4$, we first evaluate the real representative Λ_N of two-qubit subsystem $\rho_2^{(N)}$ obtained in Equation (42): We find that

$$\Lambda_N = \mathrm{diag}\left(1, 2/N, 2/N, (N-4)/N\right).$$

Eigenvalues of $G\Omega^{(N)} = G\Lambda_N G\left(\Lambda_N\right)^{\mathrm{T}}$ are given by

$$\lambda_0 = 1,\ \lambda_1 = \lambda_2 = 4/N^2,\ \lambda_3 = (N-4)^2/N^2$$

and the eigenvector

$$X_0 = (1,0,0,0)$$

corresponding to the highest eigenvalue $\lambda_0 = 1$ satisfies the relation $X_0^{\mathrm{T}} G X_0 = 1$. Thus, the semi-axes of the steering ellipsoid (see Sec. 4.2) corresponding to two-qubit subsystem density matrix $\rho_2^{(N)}$ of $\left|\mathrm{W}\overline{\mathrm{W}}\right\rangle_N$ are given by

$$a_1 = \sqrt{\frac{\lambda_1}{\lambda_0}} = \frac{2}{N} = a_2;\ a_3 = \sqrt{\frac{\lambda_3}{\lambda_0}} = \frac{N-4}{N} \tag{69}$$

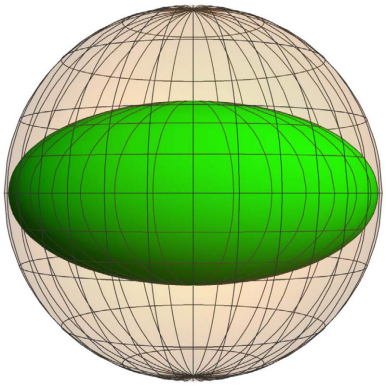

Figure 1. Oblate spheroid representing the state $\left|\mathrm{W}\bar{\mathrm{W}}\right\rangle_3$: Length of the semi-axes: $a_1 = 1$, $a_2 = a_3 = 1/2$.

Thus, the N-qubit $\mathrm{W}\bar{\mathrm{W}}$ state is represented geometrically by a spheroid ($a_1 = a_2 = 2/N$) centered at the origin of the Bloch sphere. For $N = 5$, we obtain an oblate spheroid (see **Figure 2**).

When $N = 6$, it is readily seen from Equation (69) that we have a sphere of radius 1/3 (see **Figure 3**).

For $N \geq 7$, the canonical steering ellipsoids of $\left|\mathrm{W}\bar{\mathrm{W}}\right\rangle_N$ are prolate spheroids with their radius $2/N$ decreasing with N (see **Figure 4** and **Figure 5**).

One can obtain similar canonical steering ellipsoids for generalized counterparts of GHZ and $\mathrm{W}\bar{\mathrm{W}}$ states by constructing the real representatives of their two-qubit subsystems. We notice that the nature of the canonical ellipsoids remain the same as that for $\left|\mathrm{W}\bar{\mathrm{W}}\right\rangle_N$ and $\left|\mathrm{GHZ}\right\rangle_N$ but the volume of the ellipsoid increases when $\theta < \pi/2$, $\theta > \pi/2$. This indicates the increase in shareability of entanglement among its subsystems. Quite in accordance with increase in pairwise entanglement (concurrence) and decrease in monogamous nature (decrease in concurrence tangle) of these states (see Sec. 3), their shareability of entanglement decreases when $\theta > \pi/2$, $\theta < \pi/2$ as reflected through the volume of the corresponding canonical steering ellipsoids.

6. Volume Monogamy Features of $\left|\mathrm{W}\bar{\mathrm{W}}\right\rangle_N$ and $\left|\mathrm{GHZ}\right\rangle_N$

The restriction on shareability of quantum correlations in a multipartite state get captured in various monogamy relations, which find interesting applications in ensuring security in quantum key distribution [34] [35]. A geometrically intuitive monogamy relation in terms of the volumes of the steering ellipsoids representing the two-qubit subsystems of multiqubit pure states has been proposed and extensively studied in Refs. [16] [17] [18] [19]. The volume monogamy relation is stronger than the well-known Coffman-Kundu-Wootters monogamy relation given by Equation (45) and is applicable to N-qubit pure states.

The normalized volume v_N of the quantum steering ellipsoid corresponding to pure symmetric N-qubit state $\left|\Psi\right\rangle_{\mathrm{sym}}$ is given by [26]

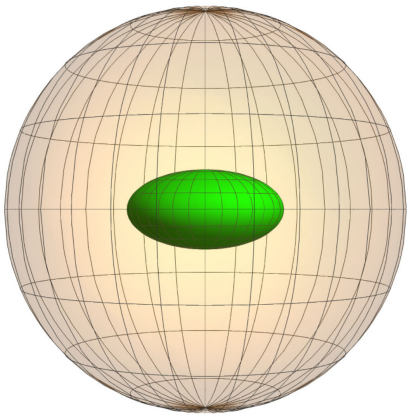

Figure 2. Canonical steering ellipsoid representing $\left|W\bar{W}\right\rangle_5$ with semiaxes $a_1 = a_2 = 2/5$, $a_3 = 1/5$.

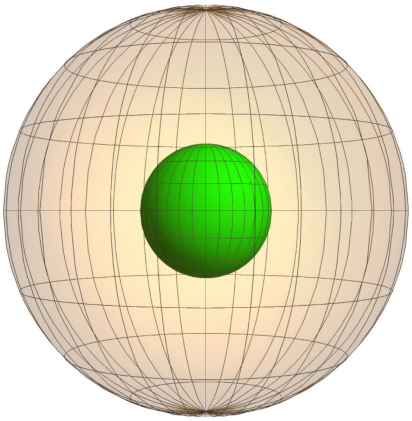

Figure 3. Sphere of radius 1/3, the canonical steering ellipsoid of $\left|W\bar{W}\right\rangle_6$.

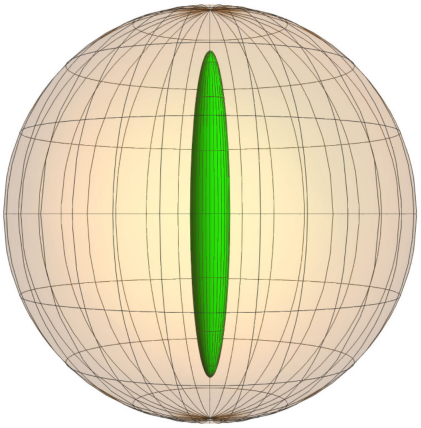

Figure 4. Prolate spheroid with semiaxes $a_1 = a_2 = \frac{1}{10}$, $a_3 = \frac{4}{5}$ representing $\left|W\bar{W}\right\rangle_{20}$.

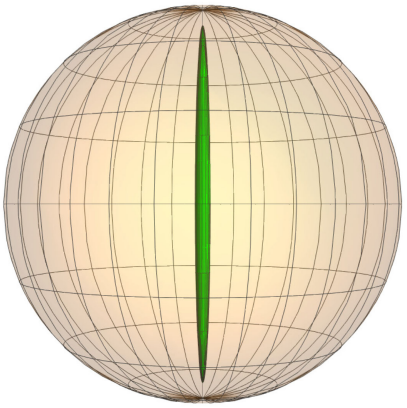

Figure 5. Prolate spheroid with semiaxes $a_1 = a_2 = 1/25$, $a_3 = 23/25$ representing $\left|W\bar{W}\right\rangle_{50}$.

$$v_N = \frac{\left|\det \Lambda_N\right|}{\left(1-r^2\right)^2} \tag{70}$$

Here Λ_N is the real representative of the two-qubit density matrix $\rho_2^{(N)}$ of $\left|\Psi\right\rangle_{\text{sym}}$ and $\vec{r} = (r_1, r_2, r_3)$ ($|\vec{r}| \le 1$) is the Bloch-vector of the single qubit subsystem. It has been shown in [26] that the volume monogamy relation in the state $\left|\Psi\right\rangle_{\text{sym}}$ is given by

$$\left(v_N\right)^{\frac{2}{3}} \le \frac{1}{2}. \tag{71}$$

We proceed to study the volume monogamy relation governing N-qubit $W\bar{W}$ state. The LHS of the monogamy inequality (71) is a measure of the degree of restriction on shareability of quantum correlations in any arbitrary N-qubit pure symmetric state. The lowest possible value 0 indicates maximum restriction on shareability of entanglement. Equality sign in (71) indicates least restriction and largest allowed shareability of entanglement.

For $N = 3$, the real representative Λ_3 of the two-qubit subsystem $\rho_2^{W\bar{W}}$ of $\left|W\bar{W}\right\rangle_3$ is given in Equation (64). It is seen that the Bloch vector components $r_1 = 2/3$, $r_2 = r_3 = 0$ (see Equation (64)) leading to $r = \sqrt{r_1^2 + r_2^2 + r_3^2} = 2/3$. We find that $\left|\det \Lambda^{(3)}\right| = 4/81$. Thus we obtain (see Equation (70)) $v_3 = 4/25$. Thus, volume monogamy relation is readily satisfied:

$$\left(v_3\right)^{2/3} = 0.16 < 1/2.$$

For $\left|W\bar{W}\right\rangle_4$, we obtain $\det \Lambda_4 = 0$ as $\Lambda_4 = \text{diag}(1,1,0,0)$ (see Equation (67)). The volume monogamy relation is thus maximally satisfied. It may be noted that the real matrix corresponding to two-qubit subsystem of N-qubit GHZ state is given by $\Lambda_{\text{GHZ}} = \text{diag}(1,0,0,1)$ and hence, $\det \Lambda_{\text{GHZ}} = 0$ irrespective of the value N. Thus, the LHS of the volume monogamy inequality (71) takes its minimum value 0 for GHZ state, highlighting the strongest restrictions on sharability of entanglement.

Let us turn our attention to volume monogamy property of $\left|W\bar{W}\right\rangle_N$, $N > 4$. The real representative Λ_N of $\left|W\bar{W}\right\rangle_N$, $N > 4$ is a diagonal matrix

$\Lambda^{(N)} = \mathrm{diag}\left(1, 2/N, 2/N, (N-4)/n\right)$ with the magnitude of single qubit Block vector $r = \sqrt{r_1^2 + r_2^2 + r_3^2} = 0$. Substituting $\det \Lambda_N = 4(N-4)/N^3$ (see Equation (70)) we obtain the volume monogamy relation (71) for $\left|\mathrm{W}\overline{\mathrm{W}}\right\rangle_N$, $N > 4$:

$$v_N^{2/3} = \frac{\left(4(N-4)\right)^{2/3}}{N^2} \leq \frac{1}{2}. \tag{72}$$

We have plotted the LHS of volume monogamy relation (72) in **Figure 6**. It is evident from **Figure 6** that the sharability of entanglement gets restricted as number of qubits N increase and is quantified by reducing volume of the canonical steering ellipsoids On explicit evaluation of the volumes of steering ellipsoids (as a function of the parameter θ) of generalized $\mathrm{W}\overline{\mathrm{W}}$ and GHZ states, we find analogous features.

It is worth recalling here that the volume monogamy inequality for W state belonging to the family $\mathcal{D}_{N-1,1}$—which are constituted by two distinct spinors—is shown [26] to be $(N-1)^{-4/3} < 1/2$. A comparison of the LHS of monogamy relation of $\left|\mathrm{W}\overline{\mathrm{W}}\right\rangle_N$ and the W-class of states is depicted in **Figure 7**. It is seen that W states exhibit stricter volume monogamy for pairwise entanglement than $\mathrm{W}\overline{\mathrm{W}}$ states beyond $N \geq 7$ when the cross-over happens (see **Figure 7**).

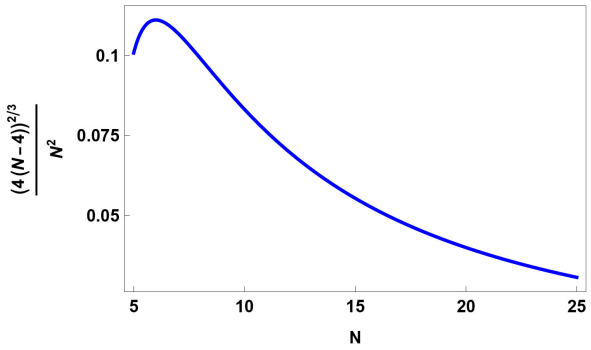

Figure 6. LHS. of the volume monogamy relation (72) obeyed by $\left|\mathrm{W}\overline{\mathrm{W}}\right\rangle_N$ state as a function of the number of qubits N.

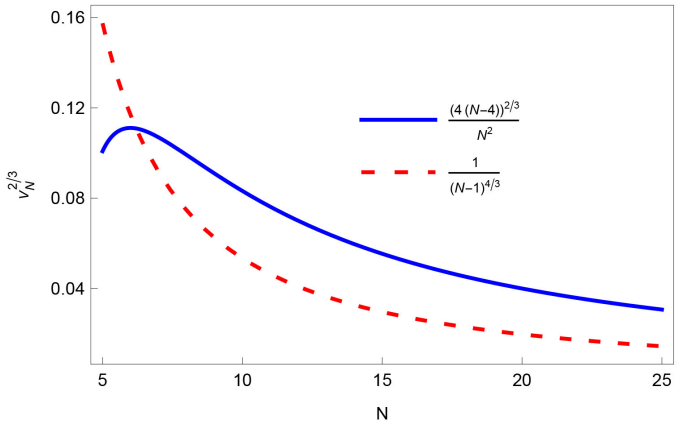

Figure 7. Comparison of the LHS of the volume monogamy relation governing $\left|\mathrm{W}\overline{\mathrm{W}}\right\rangle_N$ and the W-class of N-qubit states.

7. Summary

In this work, we have compared the features of the N-qubit GHZ and equal superposition of N-qubit W, $\overline{\mathrm{W}}$ states, which are constituted by N-distinct Majorana spinors. Such a comparison is carried out for the first time, to the best of our knowledge. We have evaluated the explicit structure of Majorana spinors of both the families. Using the structure of Majorana spinors for 3-qubit GHZ and $\mathrm{W}\overline{\mathrm{W}}$ states, we have shown that they are interconvertible under identical local operations on their qubits. Geometric visualization of N-qubit $\mathrm{W}\overline{\mathrm{W}}$ states in terms of canonical steering ellipsoids inscribed within the Bloch sphere is highlighted. Furthermore, we have investigated the volume monogamy inequality governing shareability of entanglement in N-qubit $\mathrm{W}\overline{\mathrm{W}}$ states.

Acknowledgements

ARU and Sudha are supported by the Department of Science and Technology (DST), India through Project No. DST/ICPS/QUST/2018/107. ASH is supported by the Foundation for Polish Science (IRAP Project, ICTQT, contract no. MAB/2018/5, co-financed by EU within Smart Growth Operational Programme). HSK is supported by the Institute of Information & Communications Technology Planning & 14 Evaluation (IITP) Grant funded by the Korean government (MSIT) (No. 2022-0-00463, Development of a quantum repeater in optical fiber networks for quantum internet).

Conflicts of Interest

The authors declare no conflicts of interest regarding the publication of this paper.

References

[1] Sackett, C.A., Kielpinski, D., King, B.E., Langer, C., Meyer, V., Myatt, C.J., Rowe, M., Turchette, Q.A., Itano, W.M., Wineland, D.J. and Monroe, C. (2000) Experimental Entanglement of Four Particles. *Nature* (*London*), **404**, 256-259. https://doi.org/10.1038/35005011

[2] Roos, C.F., Riebe, M., Haffner, H., Hansel, W., Benhelm, J., Lancaster, G.P.T., Becher, C., Schmidt-Kaler, F. and Blatt, R. (2004) Control and Measurement of Three-Qubit Entangled States. *Science*, **304**, 1478-1480. https://doi.org/10.1126/science.1097522

[3] Leibfried, D.G., Knill, E.H., Seidelin, S., Britton, J.W., Blakestad, B.R., Chiaverini, J., Hume, D., Itano, W.M., Jost, J.D., Langer, C., Ozeri, R., Reichle, R. and Wineland, D.J. (2005) Creation of a Six-Atom "Schrodinger Cat" State. *Nature* (*London*), **438**, 639-642. https://doi.org/10.1038/nature04251

[4] Sorensen, A., Duan, L.-M., Cirac, J.I. and Zoller, P. (2001) Many-Particle Entanglement with Bose-Einstein Condensates. *Nature* (*London*), **409**, 63-66. https://doi.org/10.1038/35051038

[5] Usha Devi, A.R., Prabhu, R. and Rajagopal, A.K. (2007) Characterizing Multiparticle Entanglement in Symmetric N-Qubit States via Negativity of Covariance Matrices. *Physical Review Letters*, **98**, Article ID: 060501. https://doi.org/10.1103/PhysRevLett.98.060501

[6] Avishai, Y. (2023) On Topics in Quantum Games. *Journal of Quantum Information Science*, **13**, 79-130. https://doi.org/10.4236/jqis.2023.133006

[7] Aloff, S., Miniere, M. and Saccoman, J. (2021) A Minimal Presentation of a Two-Generator Permutation Group on the Set of Integers. *Advances in Pure Mathematics*, **11**, 816-834. https://doi.org/10.4236/apm.2021.1110055

[8] Greenberger, D.M., Horne, M.A., Shimony, A. and Zeilinger, A. (1990) Bell's Theorem without Inequalities. *American Journal of Physics*, **58**, 1131-1143. https://doi.org/10.1119/1.16243

[9] Dicke, R.H. (1954) Coherence in Spontaneous Radiation Processes. *Physical Review*, **93**, 99-110. https://doi.org/10.1103/PhysRev.93.99

[10] Majorana, E. (1932) Atomi Orientati in Campo Magnetico Variabile. *Nuovo Cimento*, **9**, 43-50. https://doi.org/10.1007/BF02960953

[11] Bastin, T., Krins, S., Mathonet, P., Godefroid, M., Lamata, L. and Solano, E. (2009) Operational Families of Entanglement Classes for Symmetric *N*-Qubit States. *Physical Review Letters*, **103**, Article ID: 070503. https://doi.org/10.1103/PhysRevLett.103.070503

[12] Mathonet, P., Krins, S., Godefroid, M., Lamata, L., Solano, E. and Bastin, T. (2010) Entanglement Equivalence of *N*-Qubit Symmetric States. *Physical Review A*, **81**, Article ID: 052315. https://doi.org/10.1103/PhysRevA.81.052315

[13] Usha Devi, Sudha, A.R. and Rajagopal, A.K. (2012) Majorana Representation of Symmetric Multiqubit States. *Quantum Information Processing*, **11**, 685-710. https://doi.org/10.1007/s11128-011-0280-8

[14] Markham, J.H. (2011) Entanglement and Symmetry in Permutation Symmetric States. *Physical Review A*, **83**, Article ID: 042332. https://doi.org/10.1103/PhysRevA.83.042332

[15] Jevtic, S., Pusey, M.F., Jennings, D. and Rudolph, T. (2014) Quantum Steering Ellipsoids. *Physical Review Letters*, **113**, Article ID: 020402. https://doi.org/10.1103/PhysRevLett.113.020402

[16] Shi, M., Jiang, F., Sun, C. and Du, J. (2011) Geometric Picture of Quantum Discord for Two-Qubit Quantum States. *New Journal of Physics* **13**, Article ID: 073016. https://doi.org/10.1088/1367-2630/13/7/073016

[17] Shi, M., Yang, W., Jiang F. and Du, J. (2011) Quantum Discord of Two-Qubit Rank-2 States. *Journal of Physics A*: *Mathematical and Theoretical*, **44**, Article ID: 415304. https://doi.org/10.1088/1751-8113/44/41/415304

[18] Milne, A., Jevtic, S., Jennings, D., Wiseman, H. and Rudolph, T. (2014) Quantum Steering Ellipsoids, Extremal Physical States and Monogamy. *New Journal of Physics*, **16**, Article ID: 083017. https://doi.org/10.1088/1367-2630/16/8/083017

[19] Milne, A., Jennings, D., Jevtic, S. and Rudolph, T. (2014) Quantum Correlations of Two-Qubit States with One Maximally Mixed Marginal. *Physical Review A*, **90**, Article ID: 024302. https://doi.org/10.1103/PhysRevA.90.024302

[20] Cheng, S., Milne, A., Hall, M.J.W. and Wiseman, H.M. (2016) Volume Monogamy of Quantum Steering Ellipsoids for Multiqubit Systems. *Physical Review A*, **94**, Article ID: 042105. https://doi.org/10.1103/PhysRevA.94.042105

[21] Coffman, V., Kundu, J. and Wootters, W.K. (2000) Distributed Entanglement. *Physical Review A*, **61**, Article ID: 052306. https://doi.org/10.1103/PhysRevA.61.052306

[22] Verstraete, F., Dehaene, J. and DeMoor, B. (2001) Local Filtering Operations on Two Qubits. *Physical Review A*, **64**, 010101(R). https://doi.org/10.1103/PhysRevA.64.010101

[23] Verstraete, F. (2002) Quantum Entanglement and Quantum Information. Ph.D. Thesis, Katholieke Universiteit Leuven, Leuven.

[24] Sudha Karthik, H.S., Pal, R., Akhilesh, K.S., Ghosh, S., Mallesh, K.S. and Usha Devi, A.R. (2020) Canonical Forms of Two-Qubit States under Local Operations. *Physical Review A*, **102**, Article ID: 052419. https://doi.org/10.1103/PhysRevA.102.052419

[25] Anjali, K., Reena, I., Sudha Divyamani, B.G., Karthik, H.S., Mallesh, K.S. and Usha Devi, A.R. (2022) Geometric Picture for SLOCC Classification of Pure Permutation Symmetric Three-Qubit States. *Quantum Information Processing*, **21**, 326. https://doi.org/10.1007/s11128-022-03665-9

[26] Divyamani, B.G., Reena, I., Panigrahi, P.K., Usha Devi, A.R. and Sudha (2023) Canonical Steering Ellipsoids of Pure Symmetric Multiqubit States with Two Distinct Spinors and Volume Monogamy of Steering. *Physical Review A*, **107**, Article ID: 042207. https://doi.org/10.1103/PhysRevA.107.042207

[27] The Nth Roots of Any Complex Number $z = \mathrm{e}^{i\phi}$ Are Given by $z_k = \mathrm{e}^{i\phi_k}$ Where $\phi_k = \left(\frac{\phi + 2k\pi}{N}\right)$, $k = 0,1,2,\cdots,N-1$.

[28] Hill, S. and Wootters, W.K. (1997) Entanglement of a Pair of Quantum Bits. *Physical Review Letters*, **78**, 5022-5025. https://doi.org/10.1103/PhysRevLett.78.5022

[29] Wootters, W.K. (1998) Entanglement of Formation of an Arbitrary State of Two Qubits. *Physical Review Letters*, **80**, 2245-2248. https://doi.org/10.1103/PhysRevLett.80.2245

[30] Geetha, P.J., Sudha and Mallesh, K.S. (2017) Comparative Analysis of Entanglement Measures Based on Monogamy Inequality. *Chinese Physics B*, **26**, Article ID: 050301. https://doi.org/10.1088/1674-1056/26/5/050301

[31] Wong, A. and Christensen, N. (2001) Potential Multiparticle Entanglement Measure. *Physical Review A*, **63**, Article ID: 044301. https://doi.org/10.1103/PhysRevA.63.044301

[32] Li, D. (2012) The N-Tangle of Odd N Qubits. *Quantum Information Processing*, **11**, 481. https://doi.org/10.1007/s11128-011-0256-8

[33] Srinivasa Rao, K.N. (1988) The Rotation and Lorentz Groups and Their Representations for Physicists. Wiley Eastern, New Delhi.

[34] Tehral, B.M. (2004) Is Entanglement Monogamous? *IBM Journal of Research and Development*, **48**, 71-78. https://doi.org/10.1147/rd.481.0071

[35] Pawłowski, M. (2010) Security Proof for Cryptographic Protocols Based Only on the Monogamy of Bell's Inequality Violations. *Physical Review A*, **82**, Article ID: 032313. https://doi.org/10.1103/PhysRevA.82.032313